

A critical analysis of drag force modelling for disperse gas-liquid flow in a pipe with an obstacle

Tas-Köhler, S.; Liao, Y.; Hampel, U.;

Originally published:

August 2021

Chemical Engineering Science 246(2021), 117007

DOI: <https://doi.org/10.1016/j.ces.2021.117007>

Perma-Link to Publication Repository of HZDR:

<https://www.hzdr.de/publications/Publ-32503>

Release of the secondary publication
on the basis of the German Copyright Law § 38 Section 4.

CC BY-NC-ND

Chemical Engineering Science

A critical analysis of drag force modelling for disperse gas-liquid flow in a pipe with an obstacle

--Manuscript Draft--

Manuscript Number:	
Article Type:	Research paper
Section/Category:	Transport Phenomena, including Fluid Mechanics
Keywords:	CFD; bubbly flow; drag force coefficient; turbulence; vortex; hybrid drag model
Corresponding Author:	Sibel Tas-Koehler, M. Sc. Helmholtz-Zentrum Dresden-Rossendorf Dresden, Sachsen GERMANY
First Author:	Sibel Tas-Koehler, M. Sc.
Order of Authors:	Sibel Tas-Koehler, M. Sc. Yixiang Liao Uwe Hampel
Abstract:	<p>The accuracy of gas-liquid flow modelling depends on an appropriate modelling of interfacial forces. Among those, the drag is dominating. Most drag models have been derived and validated for laminar or low-turbulence flow conditions only. In this study, we evaluated different drag models from the literature for a highly turbulent gas-liquid flow around an obstacle in a pipe that produces a pronounced vortex region. We compared void fraction, as well as gas and liquid velocity profiles with experimental data obtained by means of Ultrafast X-ray Computed Tomography. We found that all the models except Bakker and Feng, predict the void fraction well compared to experimental data upstream of the obstacle, that is, for a developed two-phase pipe flow with axial symmetry. However, the void fraction downstream is grossly overestimated by all of the models. Based on the results, a hybrid drag model is proposed, which improves void fraction predictions considerably.</p>
Suggested Reviewers:	Ning Yang nyang@ipe.ac.cn Mohsen Karimi karimi@sun.ac.za Amjad Asad Amjad.Asad@imfd.tu-freiberg.de Jyeshtharaj Joshi jbj@udct.org Milton Mori mori@feq.unicamp.br Shantanu Roy roys@chemical.iitd.ac.in
Opposed Reviewers:	

- The capability of different drag models under high turbulence /vortex flow conditions is shown.
- Impacts of turbulence effects on drag modelling is presented.
- A hybrid model is proposed for high turbulence flow conditions.
- Two-phase flow hydrodynamics under complex flow conditions is analyzed.
- Phase velocities and void fraction predictions are compared with experimental data

A critical analysis of drag force modelling for disperse gas-liquid flow in a pipe with an obstacle

Sibel Tas-Koehler ^{a*}, Yixiang Liao ^a, Uwe Hampel ^{a,b}

^a Helmholtz-Zentrum Dresden-Rossendorf, Institute of Fluid Dynamics, Bautzner Landstr. 400, 01328 Dresden, Germany

^b Technische Universität Dresden, Chair of Imaging Techniques in Energy and Process Engineering, 01062 Dresden, Germany

* Corresponding author (E-mail: s.tas@hzdr.de)

ABSTRACT

The accuracy of gas-liquid flow modelling strongly depends on an appropriate modelling of interfacial forces. Among those, the drag is dominating. Most drag models reported in the literature have been derived and validated for laminar or low-turbulence flow conditions only. In this study, we evaluated different drag models from the literature for a highly turbulent gas-liquid flow around an obstacle in a pipe that produces a pronounced vortex region. We compared void fraction, as well as gas and liquid velocity profiles with experimental data obtained by means of Ultrafast X-ray Computed Tomography. We found that all the models except Bakker and Feng, predict the void fraction well compared to experimental data upstream of the obstacle, that is, for a developed two-phase pipe flow with axial symmetry. However, the void fraction downstream is grossly overestimated by all of the models. Based on the results, a hybrid drag model is proposed, which improves void fraction predictions considerably.

Keywords: CFD, bubbly flow, drag force coefficient, turbulence, vortex, hybrid drag model

Nomenclature

Latin symbols

d_B	bubble diameter [m]
C_D	drag coefficient [-]
Eo	Eötvös number [-]
F_D	drag force per unit volume [$\text{N}\cdot\text{m}^{-3}$]
k	phase indicator
M_i	source term in i -th direction [$\text{kg}\cdot\text{m}^{-2}\cdot\text{s}^{-2}$]
Mo	Morton number [-]
p	pressure [Pa]

Greek symbols

α	gas volume fraction [-]
ν	kinematic viscosity [$\text{m}^2\cdot\text{s}^{-1}$]
σ	surface tension [$\text{kg}\cdot\text{s}^{-2}$]
ε	turbulence dissipation rate [$\text{m}^2\cdot\text{s}^{-3}$]
μ	dynamic viscosity [$\text{kg}\cdot\text{m}^{-1}\cdot\text{s}^{-1}$]
$\tau_{ij}^{Lam}, \tau_{ij}^{Turb}$	laminar stress tensor [$\text{kg}\cdot\text{m}^{-1}\cdot\text{s}^{-2}$], turbulent stress tensor [$\text{kg}\cdot\text{m}^{-1}\cdot\text{s}^{-2}$]
ρ	density [$\text{kg}\cdot\text{m}^{-3}$]

Subscripts

Re	Reynolds number [-]	B	bubble
u	velocity [m·s ⁻¹]	L	liquid phase
		G	gas phase

24 Acronyms

- 25 BIT: Bubble-Induced Turbulence
 26 CFD: Computational Fluid Dynamics
 27 FAD: Favre-Averaged Drag
 28 MUSIG: Multiple Size Group Model
 29 SST: Shear Stress Transport
 30 UFXCT: Ultrafast X-ray Computed Tomography

31 1. Introduction

32 Bubbly flows are important in many fields of process, energy and environmental engineering. Examples
 33 are boiling two-phase flow in nuclear reactors (Tas-Koehler *et al.* (2020)), stirred tanks (Guan *et al.*
 34 (2020)), bubble columns (Besagni *et al.* (2018)) and airlift reactors (Jiang *et al.* (2016)). In all these
 35 applications the modelling and simulation of two-phase flow is required to understand and predict heat
 36 and mass transfer, mixing efficiency and chemical reaction (Guan *et al.* (2020); Pourtousi *et al.* (2014)).
 37 Computational fluid dynamics (CFD) has meanwhile considerably progressed to simulate two-phase
 38 flows. However, there are still major challenges with complex three-dimensional flow situations. One
 39 example is two-phase flow near impeller blades in reactors where gas accumulates in local vortex
 40 regions. Another example is flow separation behind spacers with vanes in nuclear fuel assemblies. Yet,
 41 a third example is bubble columns with internals. For all these applications, improved numerical CFD
 42 modelling is needed. Especially for the Euler-Euler CFD modelling context this requires appropriate
 43 closure equations for interfacial forces (Liao *et al.* (2018)).

44 In two-phase bubbly flow simulations, the momentum exchange between the phases is calculated via
 45 interfacial forces such as drag, lift, turbulent dispersion, wall lubrication and virtual mass. Among them,
 46 the drag force is the dominant force with a significantly higher magnitude than the other forces. Hence,
 47 accurate drag modelling is of primary importance (Chen (2004); Pourtousi *et al.* (2014); Yamoah *et al.*
 48 (2015)).

49 The interfacial drag force

$$F_D = -\frac{3 C_D}{4 d_B} \alpha \rho_L |\mathbf{u}_G - \mathbf{u}_L| (\mathbf{u}_G - \mathbf{u}_L) \quad (1)$$

50 determines the relative velocity between two phases as well as lateral migration of the gas phase. Here,
 51 d_B is the bubble diameter, α is the gas void fraction, ρ_L is the liquid density, \mathbf{u}_G is the gas velocity, \mathbf{u}_L
 52 is the liquid velocity and C_D is the drag coefficient. A large number of C_D closures have been proposed
 53 for the drag model in the literature. Most of the closures were obtained from bubble rise in stagnant
 54 liquid experiments. Schiller & Naumann (1935) developed a C_D model by considering a single and rigid
 55 sphere bubble for a wide range of Re_B

$$Re_B = \frac{\rho_L |\mathbf{u}_L - \mathbf{u}_G| d_B}{\mu_L}. \quad (2)$$

56 The Schiller&Naumann model gives good results for the small spherical bubbles (up to a diameter of
 57 2.5 mm) and the low void fraction cases. However, it does not consider the deformation of the bubbles.

58 In addition, this model uses a constant C_D for high Re_B . Morsi & Alexander (1972) correlated a C_D
 59 model for a wide range of Re_B . However, the model includes different constants for different ranges of
 60 Re_B . Grace *et al.* (1976) improved the Schiller&Naumann model by considering the bubble deformation.
 61 The Grace model bases three non-dimensional numbers: Re_B , Eötvös number (Eo)

$$Eo = \frac{g(\rho_L - \rho_G)d_B^2}{\sigma} \quad (3)$$

62 and Morton number (Mo)

$$Mo = \frac{g(\rho_L - \rho_G)\mu_L^4}{\rho_L^2\sigma^3}. \quad (4)$$

63 Similar to the Schiller&Naumann model, the Grace model is suitable for low void fraction cases. Ishii
 64 & Zuber (1979) developed C_D correlations for bubbly flow by considering also the bubble deformation.
 65 They compared the drag coefficients with experimental data and obtained satisfactory agreements in a
 66 wide range of the particle concentration and Reynolds number. Although the application range was not
 67 given explicitly, it is expected to be valid approximately for $Eo < 10^6$ and $Re_B < 10^4$ (Asad *et al.*
 68 (2017)). The main difference between the Ishii&Zuber and the Grace model is the definition of C_D for
 69 ellipsoidal bubbles ($C_{Dellipso}$). Silva *et al.* (2012) investigated the capability of the Ishii&Zuber model
 70 for the heterogeneous flow in a bubble column. They found that the Ishii&Zuber model overestimates
 71 the gas holdup compared to experimental data. Masood & Delgado (2014) compared the above drag
 72 models (Ishii&Zuber, Grace and Schiller&Naumann) and showed that while all drag models provide
 73 reasonable liquid axial velocity results compared to experiments, the model of Ishii&Zuber predicts
 74 axial gas velocity better than the other two models.
 75

76 Tomiyama *et al.* (1998) developed C_D closures from experimental data of a single bubble in a stagnant
 77 liquid that include the effects of not only fluid properties, gravity, bubble deformation but also the degree
 78 of contamination (pure, moderately contaminated and fully contaminated). The correlations depend on
 79 two non-dimensional numbers, i.e. Re_B and Eo . They are valid for $10^{-2} < Eo < 10^3$ and $10^{-3} <$
 80 $Re_B < 10^5$. Zhang & VanderHeyden (2002) developed a C_D model, which is a function of Re_B only.
 81 The range of applicability for Zhang&VanderHeyden model was not given explicitly. Simonnet *et al.*
 82 (2007) empirically derived a C_D model without bubble deformation and Re_B consideration, yet, the
 83 model includes a correction factor that is account for the influence of local void fraction. Since the
 84 Tomiyama model considers different flow properties and is applicable for high Re_B cases, it has often
 85 been compared with other models in the literature, especially for bubble columns. Zhang *et al.* (2006)
 86 compared Ishii&Zuber and Tomiyama drag models for two different square-cross sectioned bubble
 87 columns of two different aspect ratios. They found that with the Tomiyama model, the predicted slip
 88 velocity agrees well with the experimental data in both columns. Besagni *et al.* (2018) compared the
 89 Tomiyama and Grace models for small-scale and large-scale bubble columns. They found that the
 90 Tomiyama model provides a better agreement to experimental data in terms of a void fraction. Tabib *et*
 91 *al.* (2008) compared the Schiller&Naumann, Ishii&Zuber, the Grace and Zhang&VanderHeyden models
 92 to estimate the gas-liquid flow pattern in bubble columns. The results showed that whereas the
 93 predictions of the Ishii&Zuber and Zhang&VanderHeyden models are closer to experimental data for
 94 low superficial gas velocity, only the Zhang&VanderHeyden model is appropriate for predicting the
 95 flow pattern at high superficial gas velocity. Gupta & Roy (2013) investigated four drag models e.g.
 96 Schiller&Naumann, Tomiyama, Ishii&Zuber and Zhang&VanderHeyden to study gas-liquid in a bubble
 97 column. They found that all drag models provide similar axial liquid velocity predictions for low gas

98 holdup and superficial velocities. However, they underlined that further studies are necessary for higher
99 gas velocities. Jin et al. (2019) compared the drag models of Ishii&Zuber, Tomiyama, Simonnet and
100 Grace. They reported that Tomiyama gives better void fraction results compared to the experimental
101 data for medium to high Re_B number and low void fraction. Wang & Yao (2016) analysed different
102 interface force models for gas-liquid flow and found that for the low bubble Reynolds number (Re_B),
103 Schiller&Naumann, Morsi&Alexander, Grace, Tomiyama and Ishii&Zuber models provide similar
104 results in terms of radial void fraction. However, for the high Re_B , only Grace, Tomiyama and
105 Ishii&Zuber models, which consider bubble deformation, showed good accuracy. Yamoah et al. (2015)
106 numerically investigated different drag models such as Grace, Ishii&Zuber, Tomiyama and Simonnet.
107 All drag coefficient correlations provided satisfying void fraction results in comparison with
108 experimental data. Although the Tomiyama model provides good predictions for both bubble column
109 and pipe geometry, it is not the case for an external loop reactor, which has more flow complexity. Jiang
110 *et al.* (2016) investigated the performance of Tomiyama, Schiller&Naumann and dual bubble size
111 (DBS)-local model for an external loop airlift reactor. They found that the Schiller&Naumann model
112 underestimates the local gas holdup at lower superficial gas velocity whereas the Tomiyama model
113 overestimates it at higher superficial gas velocity.

114 In a turbulent flow, a bubble undergoes continuous acceleration and deceleration as well as deformation
115 due to turbulent eddies. The impact of turbulent eddies on the motion of the gas phase is generally
116 ignored by assuming a standard drag model that has been obtained in quiescent flow. Such an
117 assumption can cause considerable errors in the void fraction profile under turbulent conditions
118 (Doroodchi *et al.* (2008)). Thus, there are drag closures that consider turbulence effects in the literature.
119 Bakker & Vandenaeker (1994) attempted to describe the effect of turbulence on the drag coefficient by
120 utilizing a modified Reynolds number in a common correlation developed for stagnant fluid. Brucato *et*
121 *al.* (1998) performed experiments to measure drag coefficients of solid particles in a turbulent flow.
122 They proposed a new drag coefficient correlation based on the Tomiyama model by considering the
123 ratio of bubble diameter to the Kolmogorov length scale (based on volume-averaged energy dissipation
124 rate) of turbulence. Lane *et al.* (2002) applied the Brucato model to bubbles since the mechanism of
125 drag modification is believed to be similar and confirmed that the Brucato model can be used for the
126 bubbles. Lane *et al.* (2005) proposed a C_D model that is based on the available experimental data in the
127 literature. They found that there is a relation between the ratio of the slip velocity to the particle terminal
128 velocity and drag coefficient.

129 Khopkar & Ranade (2006) compared the drag models of Brucato and Bakker for a stirred vessel. They
130 showed that the Brucato model provides better agreement with the experimental data for the gas holdup.
131 Karimi *et al.* (2012) numerically investigated the performance of Schiller&Naumann and Lane drag
132 models in a Rushton-turbine flotation tank under turbulent conditions. They found that while the
133 Schiller&Naumann model overestimate the gas holdup compared to experimental data, the Lane model
134 provides fair agreement. Feng & Bolotnov (2016) proposed a modified version of Tomiyama model for
135 C_D based on DNS simulations. However, the model does not consider the bubble deformation. They
136 indicated that the modified model is valid for Re_B up to 900. Thus, they point out that further
137 investigations are needed to validate its applicability on higher Re_B . Salibindla et al. (2020) calculated
138 C_D of deforming bubbles in isotropic turbulence at a high-energy dissipation rate ($\varepsilon \sim 0.5 \text{ m}^2 \text{ s}^{-3}$) via
139 measurements of mean bubble and flow vertical velocity. They showed that when $Re_B < 400$, the
140 results agree well with the data of the Tomiyama model for bubbles rising in contaminated water.
141 For $Re_B > 400$, they developed a new C_D model based on a turbulence-based Weber number.
142 Mathematical descriptions of all aforementioned models are given in Table 1.

143 The literature review shows that whereas the Schiller&Naumann model predicts axial gas and liquid
144 velocities satisfactorily, yet, it underestimates the local void fraction at low superficial gas velocity, the
145 Ishii&Zuber model predicts axial gas and liquid velocities well for low void fraction and superficial
146 velocities, yet, it overestimates the void fraction. The Tomiyama model generally provides good void
147 fraction accuracy for medium to high Re_B number and low void fraction. However, when there is flow
148 complexity, the Tomiyama model overestimates the void fraction. The Brucato model predicts the void
149 fraction well at high turbulence. For the Feng and Salibindla models, investigations are still required. It
150 can be concluded that it is not clear whether available drag models are appropriate for complex two-
151 phase flow simulations. In addition, the available drag models, which are appropriate for high
152 turbulence, also need validation in the presence of a vortex region where sudden shear changes are
153 present. In this context, the aim of the study, to evaluate the capability of drag models under the high
154 turbulence-uniform/vortex flow conditions that have a more practical use for engineering applications.
155 Thus, a capability analysis of the different drag models in the Euler-Euler framework of bubbly flow
156 simulations was performed for the case of a half-obstructed pipe and two different turbulence conditions.
157 Both the capability of the most widely applied C_D models in the literature for low- and high-turbulence
158 conditions (i.e. Schiller&Naumann, Grace, Ishii&Zuber, Tomiyama) and less applied C_D models that
159 consider the turbulence effects (i.e. Bakker, Brucato, Feng and Salibindla) were investigated. Simulated
160 gas volume fraction, liquid velocity and gas velocity are compared against experimental data of
161 Neumann-Kipping *et al.* (2020).

162 Table 1: Summary of the drag closure models considered in the literature review.

Reference	Mathematical description
Schiller&Naumann model	$C_D = \begin{cases} 24(1 + 0.15Re_B^{0.687})/Re_B & Re_B \leq 1000 \\ 0.44 & Re_B > 1000 \end{cases}$
Morsi&Alexander model	$C_D = a_1 + \frac{a_2}{Re_B} + \frac{a_3}{Re_B}$ $a_1, a_2, a_3 = \begin{cases} 0, 24, 0 & 0 < Re_B < 0.1 \\ 3.69, 22.73, 0.0903 & 0.1 < Re_B < 1 \\ 1.222, 29.1667, -3.8889 & 1 < Re_B < 10 \\ 0.6167, 46.50, -116.67 & 10 < Re_B < 100 \\ 0.3644, 98.33, -2778 & 100 < Re_B < 1000 \\ 0.357, 148.62, -47500 & 1000 < Re_B < 5000 \\ 0.46, -490.546, 578700 & 5000 < Re_B < 10000 \\ 0.5191, -1662.5, 5416700 & Re_B \geq 10000 \end{cases}$
Grace model	$C_D = \max[C_{Dsphere}, \min(C_{Dellipse}, C_{Dcap})]$ $C_{Dsphere} = \begin{cases} \frac{24}{Re_B} & Re_B \leq 0.01 \\ \max\left(\frac{24}{Re_B}(1 + 0.15Re_B^{0.687}), 0.44\right) & 0.01 > Re_B \end{cases}$ $C_{Dcap} = \frac{8}{3}$, $C_{Dellipse} = \frac{4}{3} \frac{gd_B(\rho_L - \rho_G)}{U_t^2 \rho_L}$ $U_t = \frac{\mu_L}{d_B \rho_L} Mo^{-0.149}(J - 0.857)$, $J = \begin{cases} 0.94H^{0.757} & 2 < H \leq 59.3 \\ 3.42H^{0.441} & H > 59.3 \end{cases}$, $H = \frac{4}{3} Eo Mo^{-0.149} \left(\frac{\mu_L}{9 \times 10^{-4}}\right)^{-0.14}$
Ishii&Zuber model	$C_D = \max[C_{Dsphere}, \min(C_{Dellipse}, C_{Dcap})]$ spherical regime $0 \leq Re_B < 1000$, ellipse and cap regime $Re_B > 1000$
Bakker model	$C_D = \frac{24}{Re_B^2} (1 + 0.15Re_B^{0.687})$, $Re_B^* = \frac{\rho_L \mathbf{u}_L - \mathbf{u}_G d_B}{\mu_L + \frac{2}{9} \mu_t}$

$$C_D = \max \left[\min \left(\frac{16}{Re_B} (1 + 0.15 Re_B^{0.687}), \frac{48}{Re_B}, \frac{8Eo}{3(Eo + 4)} \right), \frac{8Eo}{3(Eo + 4)} \right] \text{ (pure)}$$

Tomiyama model $C_D = \max \left[\min \left(\frac{24}{Re_B} (1 + 0.15 Re_B^{0.687}), \frac{72}{Re_B}, \frac{8Eo}{3(Eo + 4)} \right), \frac{8Eo}{3(Eo + 4)} \right] \text{ (moderately contaminated)}$

$$C_D = \max \left[\left(\frac{24}{Re_B} (1 + 0.15 Re_B^{0.687}) \right), \frac{8Eo}{3(Eo + 4)} \right] \text{ (fully contaminated)}$$

Brucato model $\frac{C_D - C_{D0}}{C_{D0}} = 6.5 \times 10^{-6} \left(\frac{d_B}{\lambda} \right)^3, \quad \lambda = \left(\frac{\nu^3}{\varepsilon} \right)^{1/4}, \quad C_{D0} = \max \left[\left(\frac{24}{Re_B} (1 + 0.15 Re_B^{0.687}) \right), \frac{8Eo}{3(Eo + 4)} \right]$

Zhang&VanderHeyden model $C_D = 0.44 + \frac{24}{Re_B} + \frac{6}{1 + \sqrt{Re_B}}$

Lane model $\frac{C_D}{C_{D0}} = \left(\frac{U_S}{U_T} \right)^{-2}, \quad \frac{U_S}{U_T} = 1 - 1.4 \left(\frac{\tau_B}{T_L} \right)^{0.7} \exp \left(-0.6 \left(\frac{\tau_B}{T_L} \right) \right), \quad \tau_B = \frac{U_T}{2g}, \quad T_L = 0.135 \frac{k}{\varepsilon}$

$$C_D = C_{D\infty} E_\infty, \quad C_{D\infty} = \frac{4}{3} \frac{\rho_L - \rho_G}{\rho_L} g d_B \frac{1}{U_t^2}, \quad U_t = \frac{u_{b1} u_{b2}}{\sqrt{u_{b1}^2 + u_{b2}^2}}, \quad u_{b1} = \frac{1}{18} \frac{\rho_L - \rho_G}{\mu_L} g d_B^2 \left(\frac{3\mu_G + 3\mu_L}{3\mu_G + 2\mu_L} \right),$$

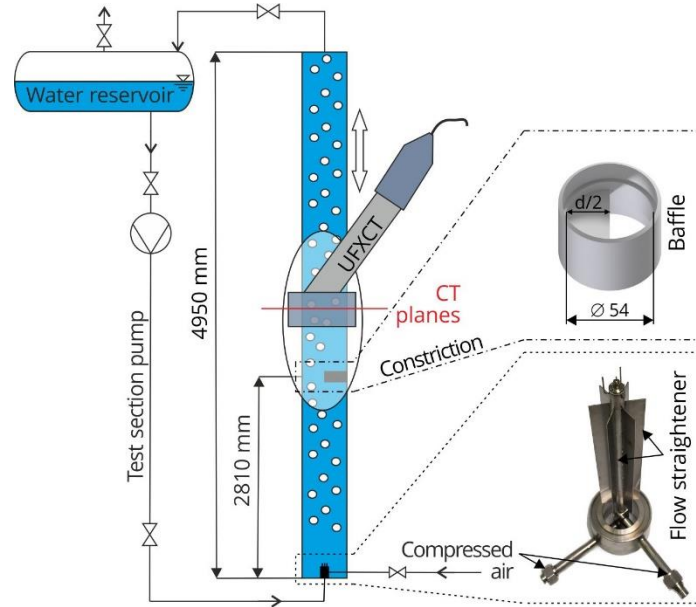
Simonnet model $u_{b2} = \sqrt{\frac{2\sigma}{(\rho_L - \rho_G) d_B} + \frac{g d_B}{2}}, \quad E_\infty = (1 - \alpha_G) \left[(1 - \alpha_G)^m + \left(4.8 \frac{\alpha_G}{1 - \alpha_G} \right)^m \right]^{-2/m}, \quad m = 25$

Feng model $C_D = \min \left[\frac{16}{Re_B} (1 + 0.15 Re_B^{0.687}), \frac{48}{Re_B} (1 + 3 \times 10^{-10} Re_B^{3.3189}) \right]$

Salibindla model $C_D = \max \left(\frac{24}{Re_B} (1 + 0.15 Re_B^{0.687}), \min(f(Eo), f(Eo)/We^{1/3}) \right), \quad f(Eo) = \frac{8Eo}{3(Eo+4)}, \quad We = 2.13 \rho (\varepsilon d_B)^{2/3} d_B / \sigma$

164 **2. Experimental setup**

165 Numerical results were compared against experimental data of Neumann-Kipping *et al.* (2020). The
 166 experiments were carried out at a vertical pipe of 4950 mm height and 54 mm inner diameter (Fig.1). A
 167 semi-circular obstacle that blocks half of the inner pipe cross-section was used to generate a vortex
 168 region. During the experiment, water was circulated upwards through the pipe and air was injected via
 169 a gas injection module from the bottom of the pipe at 4 bar and 30°C. Two test cases with different
 170 liquid velocities are considered (Table 2).



171
 172 Figure 1: Schematic representations of the vertical test section (left) with details of the gas injection module
 173 (bottom right) and the flow obstacle for generation of three-dimensional flow fields (top right) (Tas-Koehler et
 174 al. (2021)).

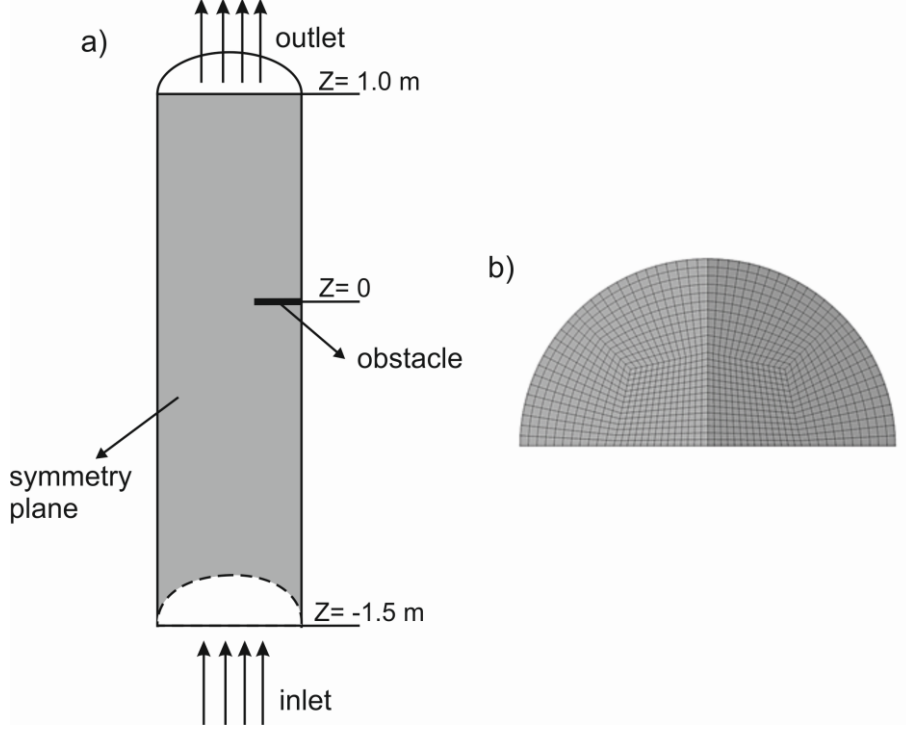
175 Table 2: Experimental operating conditions based on combinations of liquid and gas superficial velocities.

Test case	j_l [$\text{m}\cdot\text{s}^{-1}$]	j_g [$\text{m}\cdot\text{s}^{-1}$]
072	0.4050	0.0368
074	1.0170	0.0368

176 Ultrafast X-ray computed tomography (UFXCT) was applied to obtain the local gas and liquid
 177 distribution. This technique provides detailed data on the flow structure with a high resolution in space
 178 and time. For details on the experiments and data evaluation, the interested reader is referred to
 179 Neumann-Kipping *et al.* (2020) and Tas-Koehler *et al.* (2021).

180 **3. Numerical setup**

181 In the present work, the same numerical setup as already reported in Tas-Koehler *et al.* (2021) was used.
 182 3D steady state simulations with an Eulerian-Eulerian two-fluid model were carried out using ANSYS
 183 CFX 19.2. The fluid domain was modelled from 1.5 m upstream to 1 m downstream of the obstacle
 184 (Fig.2a). The details of geometry and boundary conditions can be found in Tas-Koehler *et al.* (2021).
 185 Based on grid independence study performed by Tas-Koehler *et al.* (2021), the computational domain
 186 was discretized into 252,000 hexagonal elements (Fig.2b).



187

188

Figure 2: Schematic view of a) geometry and b) mesh (Tas-Koehler et al. (2021)).

189 In the Eulerian-Eulerian two-fluid model (Yeoh & Tu (2009)) computes the phasic concentration,
 190 pressure and velocity fields by solving the continuity equation

$$\frac{\partial(\alpha_k \rho_k)}{\partial t} + \frac{\partial}{\partial x_i} (\alpha_k \rho_k \mathbf{u}_{i,k}) = 0 \quad (5)$$

191 and the momentum equation

$$\begin{aligned} \frac{\partial}{\partial t} (\alpha_k \rho_k \mathbf{u}_{i,k}) + \frac{\partial}{\partial x_i} (\alpha_k \rho_k \mathbf{u}_{i,k} \mathbf{u}_{j,k}) \\ = -\alpha_k \frac{\partial p_k}{\partial x_i} + \frac{\partial}{\partial x_j} [\alpha_k (\tau_{ij,k}^{Lam} + \tau_{ij,k}^{Turb})] + \alpha_k \rho_k \mathbf{g}_i + \mathbf{M}_{i,k}, \end{aligned} \quad (6)$$

192 here for adiabatic conditions. Thereby, k is the phase indicator, α is the volume fraction, ρ is the density,
 193 \mathbf{u}_i is the velocity component in the i -th direction, p is the pressure, τ_{ij}^{Lam} is the laminar stress tensor,
 194 τ_{ij}^{Turb} is the turbulence stress tensor and \mathbf{M}_i is the source term in the i -th direction, which includes the
 195 interfacial forces i.e. drag force, lift force, wall lubrication force, turbulent dispersion force and virtual
 196 mass force. Mathematical expressions for the individual forces are to be found in Tas-Koehler *et al.*
 197 (2021). The focus of the current work is on the drag force. All closures for interfacial forces, Bubble-
 198 Induced Turbulence (BIT) as well as breakup and coalescence models are summarized in Table 3.

199

Table 3: Applied models in the simulations.

	Term	Reference
Interfacial force	Drag	Schiller & Naumann (1935)
		Grace <i>et al.</i> (1976)

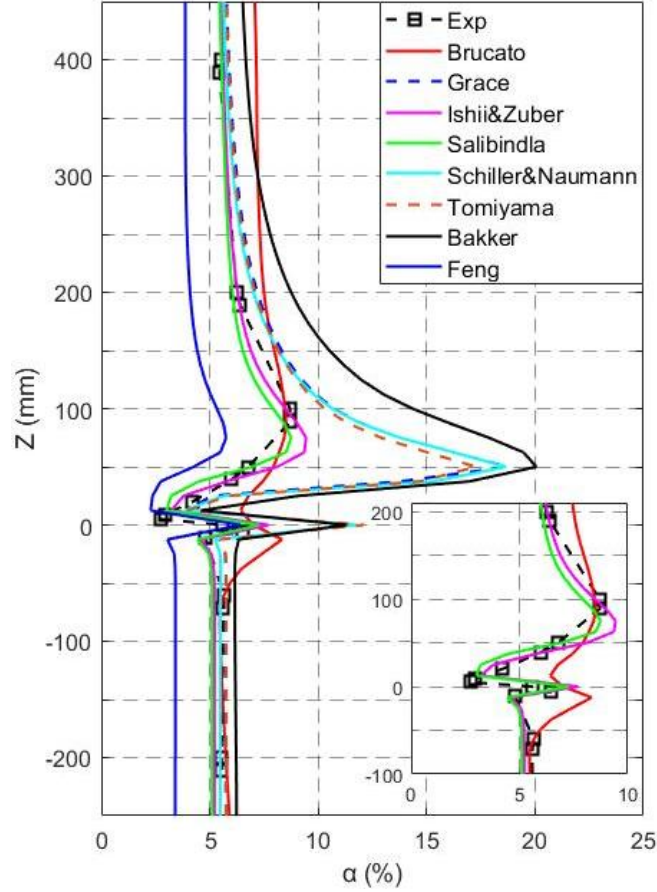
		Ishii & Zuber (1979)
		Bakker & Vandenakker (1994)
		Tomiyama <i>et al.</i> (1998)
		Brucato <i>et al.</i> (1998)
		Feng & Bolotnov (2016)
		Salibindla <i>et al.</i> (2020)
	Lift	Tomiyama <i>et al.</i> (2002)
	Turbulent dispersion	Burns <i>et al.</i> (2004)
	Wall lubrication	Hosokawa <i>et al.</i> (2002)
	Virtual mass	Auton <i>et al.</i> (1988), $C_{VM} = 0.5$
Turbulence	Liquid	Shear Stress Transport (SST), Menter (1994)
	BIT	Ma <i>et al.</i> (2017)
Population balance model	Coalescence and breakup	MUSIG model, Liao <i>et al.</i> (2015)

200 4. Results

201 4.1 Performance of existing models

202 Figure 3 shows the development of cross-section averaged gas fraction in the axial direction of the pipe
203 and different drag coefficient models for the test case 072. Up to $Z = -50$ mm, the Feng model largely
204 and the Ishii&Zuber and Salibindla models slightly underestimate the void fraction, the Bakker, the
205 Grace, the Tomiyama, the Brucato models slightly overestimate the void fraction and the
206 Schiller&Naumann model predicts the void fraction very well compared to experiments. The common
207 point of these models that provide satisfied void fraction estimations i.e. the Ishii&Zuber model, the
208 Bakker model, the Grace model, the Tomiyama model and the Brucato model is that they are based on
209 the same equation (the model of Ishii&Zuber is slightly different)

$$C_D = \left(\frac{24}{Re_b} (1 + 0.15Re_b^{0.687}) \right). \quad (7)$$



210

211 Figure 3: Cross-sectional averaged void fraction along the axial direction for the test 072.

212 The Bakker model which uses Eq.7, yet, with a different bubble Reynolds number

$$Re_b^* = \frac{\rho_L |\mathbf{u}_L - \mathbf{u}_G| d_b}{\mu_L + \frac{2}{9} \mu_t} \quad (8)$$

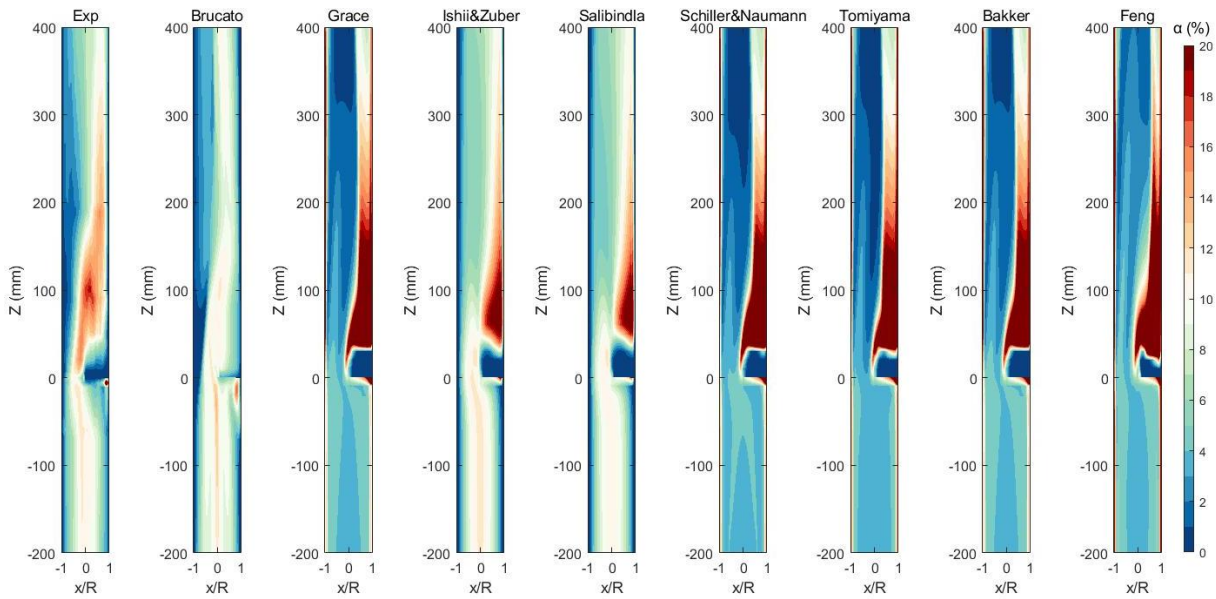
213 considers the turbulence effect via viscosity. However, it does not improve the results compared to
 214 Schiller&Naumann, Grace, Tomiyama, Salibindla and Brucato. It implies that the effect of turbulence
 215 is negligible far upstream the obstacle.

216 For $-50 \text{ mm} < Z < 0 \text{ mm}$, the Salibindla and Ishii&Zuber model provides the best void fraction
 217 estimations compared to the other models. As shown in Table 1, the Salibindla model takes into account
 218 turbulence-induced drag reduction via the Weber number, while the Ishii&Zuber model accounts for
 219 elliptical and cap bubble regimes in addition to the spherical one. The findings evidence that as the flow
 220 approaches the obstacle, turbulence and bubble deformation plays an increasingly important role. For
 221 the obstacle downstream, the Feng model again highly underestimates the void fraction as it does
 222 upstream the obstacle. The Bakker model estimates the void fraction between $0 < Z < 100 \text{ mm}$ 2.5
 223 times higher compared to the experiments.

224 For $0 < Z < 200 \text{ mm}$, the Tomiyama, the Grace, the Schiller&Naumann and Brucato models
 225 overestimate the void fraction. However, the Brucato model predicts void fraction peak around $Z =$
 226 100 mm well. The Ishii&Zuber and Salibindla models provide the best void fraction prediction here.
 227 For $200 \text{ mm} < Z < 400 \text{ mm}$, the Ishii&Zuber and Salibindla models still predict the void fraction well
 228 while the difference between these two and Tomiyama, Grace, Schiller&Naumann models reduces as Z

229 increases. After $Z = 300$ mm, all these five models predict the void fraction well compared to
 230 experiments, which is similar to the results in the far-upstream section. The analysis gives evidence that
 231 the modelling performance is significantly affected by the obstacle. Nevertheless, for the test case 072
 232 with a superficial liquid velocity of 0.4050 m/s, the Ishii&Zuber and Salibindla is capable of reproducing
 233 the average void fraction along the whole flow path, which was also confirmed by the previous study
 234 Tas-Koehler *et al.* (2021).

235 Figure 4 shows the local distribution of void fraction obtained with the different drag models. In line
 236 with Figure 3, the Ishii&Zuber, the Salibindla and Brucato models calculate the void fraction distribution
 237 well upstream the obstacle. Downstream, the experiment shows a strong gas accumulation (around 16%
 238 void fraction) directly behind the obstacle. The Grace, the Schiller&Naumann, the Tomiyama, the
 239 Bakker and Feng models predict around 20% higher in this region. For the Ishii&Zuber and Salibindla
 240 models, the prediction is better. The Brucato model predicts the distribution of the void fraction well.
 241 Yet, it cannot qualitatively capture the high amount of void fraction that is between $0 < Z < 200$ mm.



242

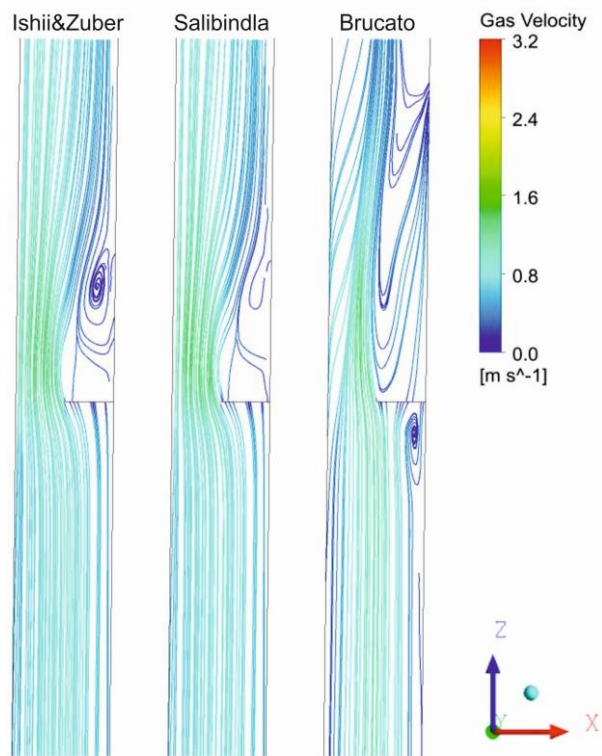
243

Figure 4: Void fraction for the test 072.

244 As can be seen from Figures 3 and 4, the Ishii&Zuber and Salibindla models provide similar results,
 245 which are satisfying compared to experiments both up- and downstream the obstacle. The Brucato model
 246 predicts the upstream well, yet, there is a difference downstream. Although the Brucato model has the
 247 capability to capture the location of the void fraction peak that is around $Z = 100$ mm, it overestimates
 248 the averaged void fraction near and downstream the obstacle.

249 Figure 5 shows streamlines of the gas velocity for $-200 \text{ mm} < Z < 200$ mm. Unlike the Ishii&Zuber
 250 and Salibindla, the Brucato model is able to predict a small vortex region upstream that leads to a very
 251 small near-wall maximum void fraction region underneath the obstacle. For the obstacle downstream, a
 252 vortex region appears after the obstacle. The bubbles are captured by this vortex resulting in a high void
 253 fraction here. However, the point is that the shape of the vortex region changes with the drag coefficient
 254 model. The Ishii&Zuber model predicts a more remarkable vortex region compared to Salibindla, which
 255 causes higher void accumulation. The Brucato model predicts a relatively large vortex region compared
 256 to other models. This relatively large vortex region causes a better fit of the void distribution as can be
 257 seen in Figure 4.

258



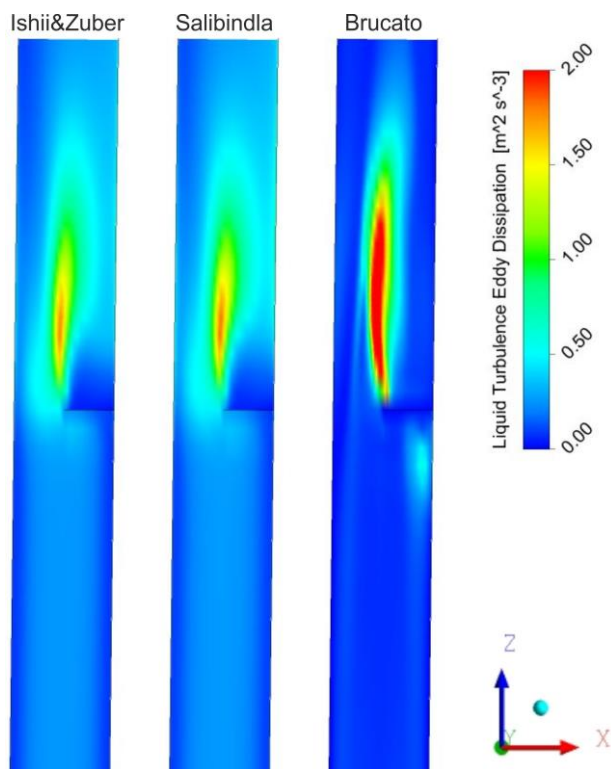
259 Figure 5: Streamlines for three different drag models: Ishii&Zuber, Salibindla and Brucato for the test 072.

260 Figure 6 presents the eddy dissipation predictions of Ishii&Zuber, Salibindla and Brucato models. In all
261 three models, the eddy dissipation difference between up- and downstream is obvious: eddy dissipation
262 remarkably increases at downstream the obstacle due to the vortex structure. Referring to Table 1, the
263 common point of the Brucato and Salibindla models is that both models are the modified version of the
264 Tomiyama model (fully contaminated) considering eddy dissipation. While the Tomiyama model
265 overestimates the void fraction in $-200 \text{ mm} < Z < 200 \text{ mm}$, the good predictions of the Brucato and
266 Salibindla models show that it is necessary to consider the eddy dissipation impact on the drag model
267 when it exceeds a certain value. According to both models, the drag coefficient may increase with the
268 dissipation rate.

269

270

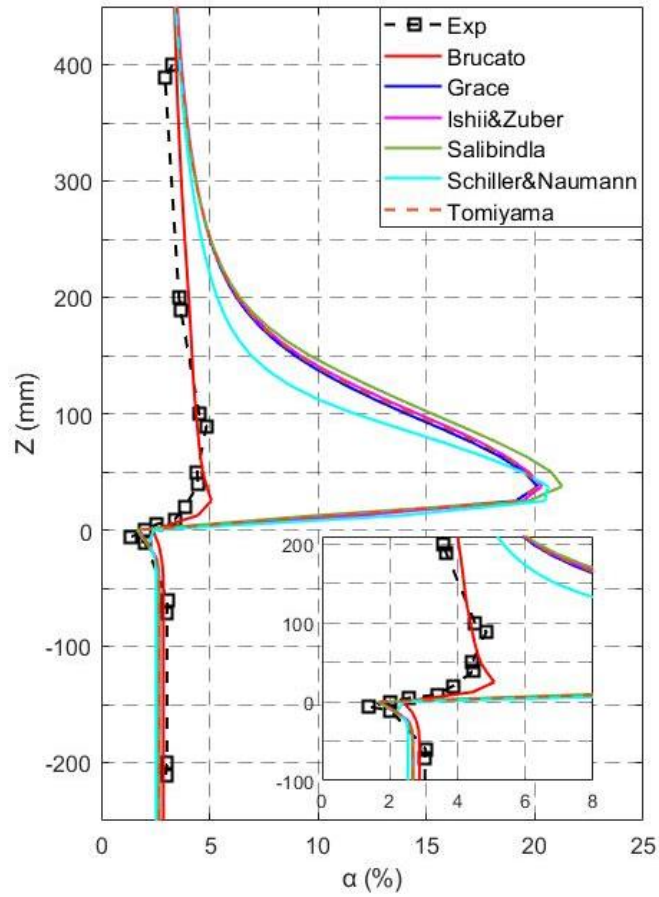
271



272

273 Figure 6: Turbulence eddy dissipation for three different drag models: Ishii&Zuber, Salibindla and Brucato for
 274 the test 072.

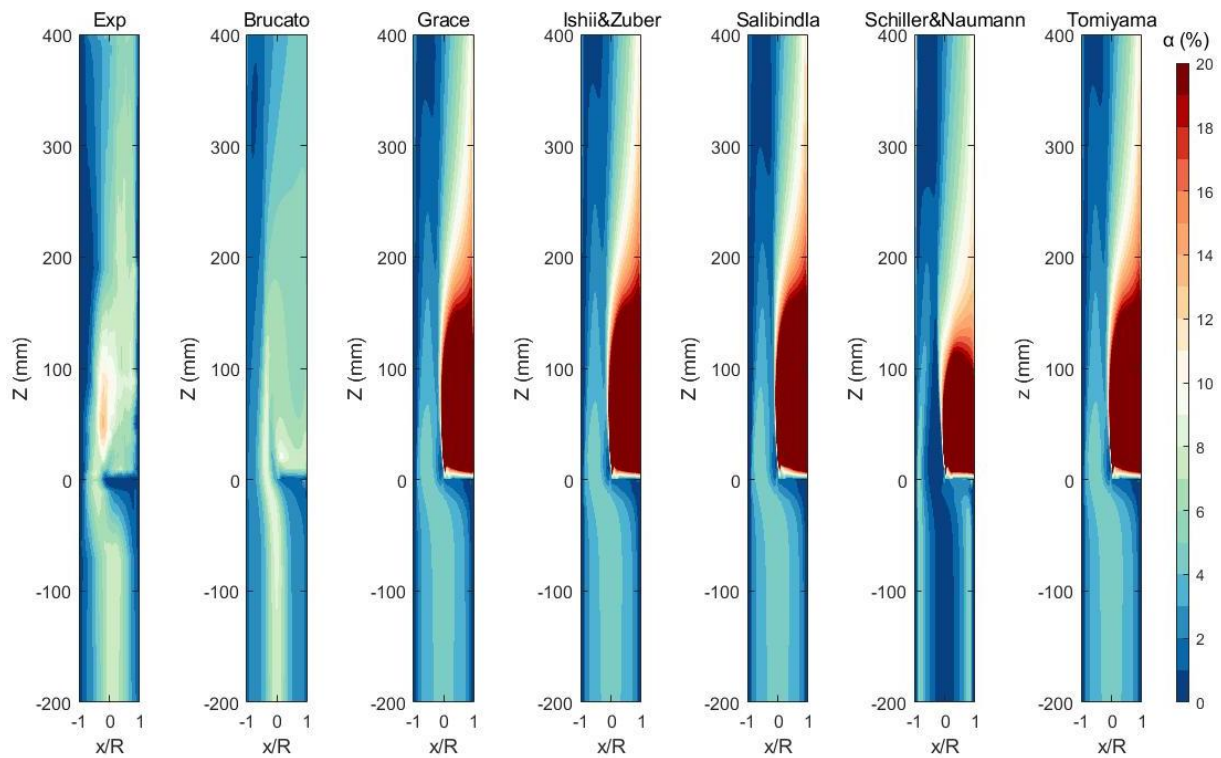
275 Now we look at test case 074 with higher liquid velocity. Here, the simulations were very unstable for
 276 the Bakker and Feng models. Thus, convergence was not achieved for these two models. Figure 7 shows
 277 averaged void fraction along the axial direction. Upstream the obstacle, all the drag models, i.e. Brucato,
 278 Grace, Ishii&Zuber, Salibindla, Schiller&Naumann and Tomiyama, slightly underestimate the void
 279 fraction compared to experiments, whereby the Brucato model provides the best void prediction. In the
 280 region just before the obstacle, the Grace model, the Ishii&Zuber model, the Salibindla model and the
 281 Tomiyama model predict the void fraction slightly better. Downstream the obstacle, all the drag models
 282 except Brucato highly overestimate the void fraction compared to the experiments. This overestimation
 283 can also be seen in Figure 8. Only the Brucato model provides satisfying void fraction results
 284 downstream the obstacle. This can be explained with reference to Figure 9. In line with Figure 6, the
 285 eddy dissipation increases at downstream the obstacle. However, it also largely increases for test case
 286 074 compared to case 072. Thus, it is even more necessary to consider the impact of turbulence for the
 287 drag model.



288

289

Figure 7: Cross-sectional averaged void fraction along the axial direction for the test 074.



290

291

Figure 8: Void fraction for the test 074.

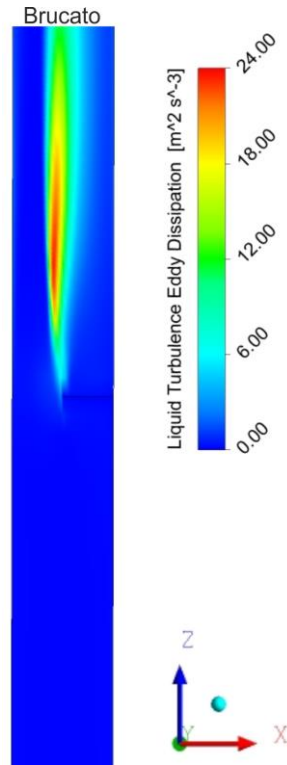


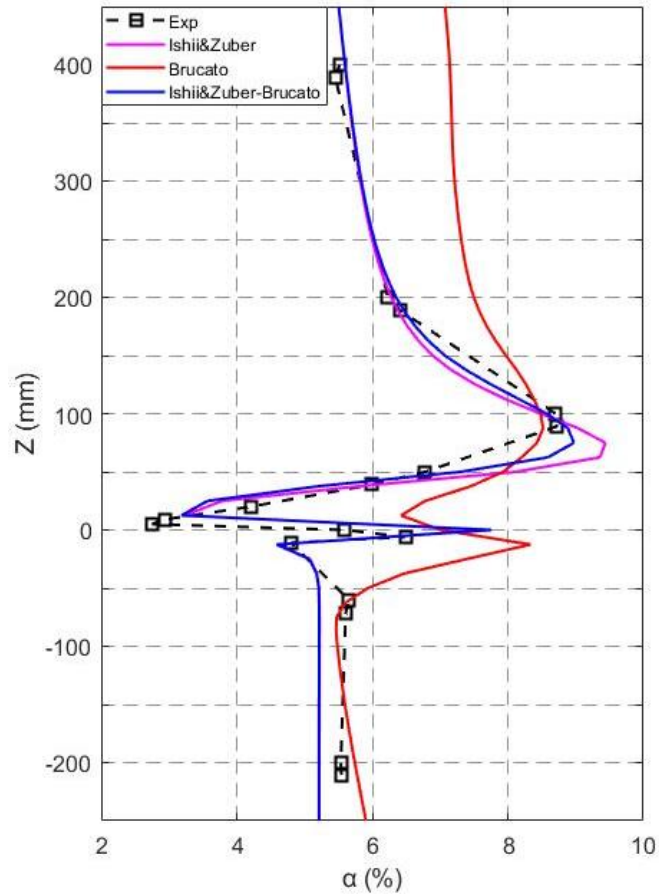
Figure 9: Turbulence eddy dissipation for Brucato model for test 074.

4.2 A hybrid drag model

As a conclusion it can be stated that in the presence of vortex region, i.e. a sudden change of eddy dissipation in the flow field, the Ishii&Zuber model prediction can be improved by taking into account the impact of turbulence effects on the drag model. Thus, a new hybrid model is proposed. According to this hybrid model, the Ishii&Zuber model is used up to a certain eddy dissipation limit ε_L . When the eddy dissipation value exceeds this limit, the simulation switches to the Brucato model. That is

$$C_D = \text{Ishii\&Zuber } \varepsilon < \varepsilon_L \text{ and Brucato else.} \quad (9)$$

As a first step, this threshold value was taken as $\varepsilon_L = 1.8 [m^2 s^{-3}]$ considering on the eddy dissipation distribution that is shown in Figure 6. Figure 10 presents the comparison of the Ishii&Zuber model, the Brucato model and the hybrid model for the test case 072. As shown in the figure, the hybrid model improves the void fraction prediction between around $50 \text{ mm} < Z < 200 \text{ mm}$ where relatively high eddy dissipation compared to upstream is observed. After the hybrid model was found to improve the simulations, different threshold values were simulated to obtain the best agreement with the measurements. Figure 11 presents the void fraction profiles for selected different threshold values i.e. $\varepsilon_L = 0.5, \varepsilon_L = 1.0, \varepsilon_L = 1.5, \varepsilon_L = 1.8$ and $\varepsilon_L = 2.0 [m^2 s^{-3}]$. Upstream the obstacle, all the threshold values provide the same void fraction predictions since the eddy dissipation value is very low. Downstream the obstacle, the threshold value that best matches the experiments is the $\varepsilon_L = 1.5 [m^2 s^{-3}]$. Thus, $\varepsilon_L = 1.5 [m^2 s^{-3}]$ was used for the rest of the study.



315

316
317

Figure 10: Comparison of cross-sectional averaged void fraction along the axial direction for Ishii&Zuber, Brucato and hybrid model for the test 072.

318

319

320

321

322

323

324

325

326

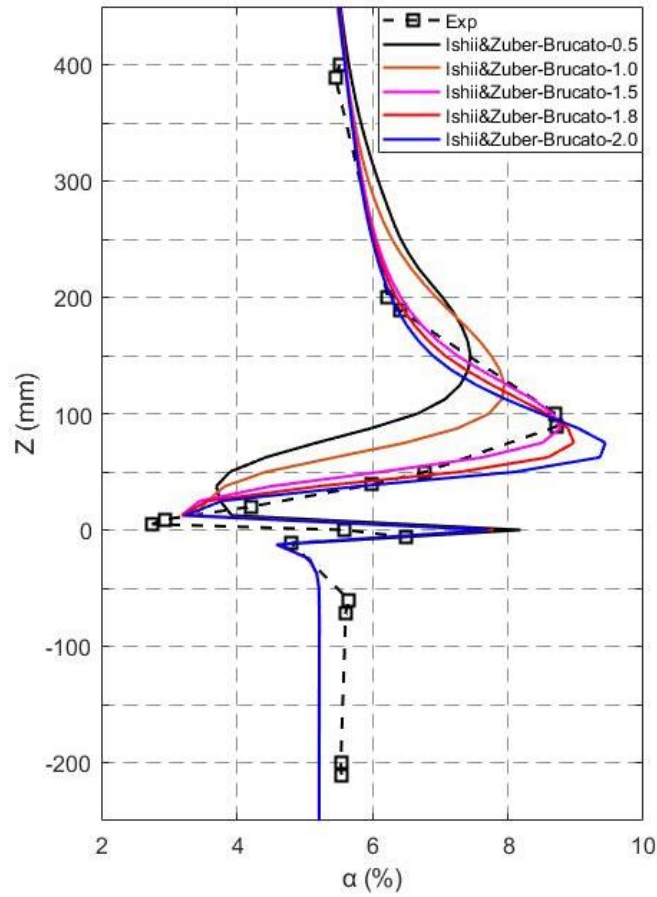
327

328

329

330

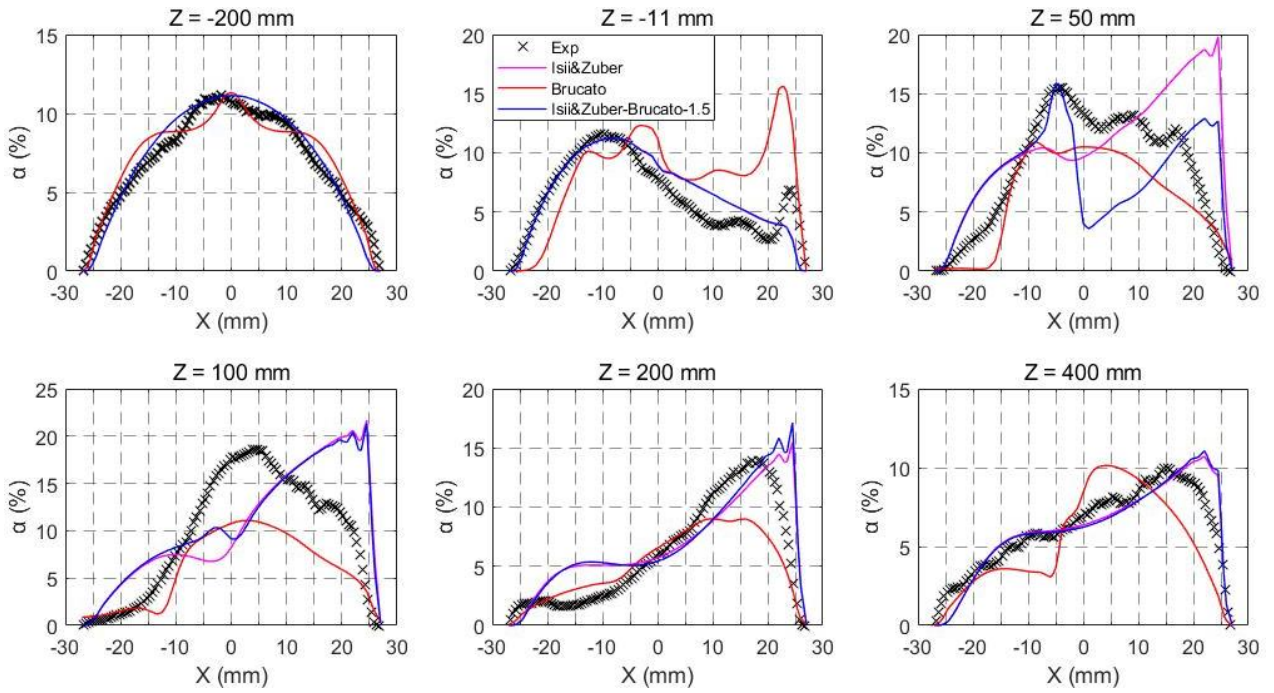
Figure 12 shows radial void distributions for Ishii&Zuber, Brucato and the hybrid model at different cross-sections for the test case 072. For $Z = -200$ mm, the Brucato model gives a slightly different void prediction compared to Ishii&Zuber and hybrid model, which provide the same results. For $Z = -11$ mm (just before the obstacle), Brucato underestimates and overestimates the void fraction for the right and left side of the pipe respectively whereas Ishii&Zuber and hybrid models predict well. For $Z = 50$ mm (where the vortex structure starts to occur), Ishii&Zuber and hybrid models slightly overestimate the void fraction up to $X = -10$ mm while the Brucato model slightly underestimates it. The hybrid model improves the void fraction prediction between -10 mm $< X < 2$ mm. After $X = 2$ mm, Ishii&Zuber and hybrid models provide different void estimations, which are unsatisfactory. The Brucato model generally underestimates the void fraction except in the area -5 mm $< X < -10$ mm. For $Z = 100$ mm, $Z = 200$ mm and $Z = 400$ mm, the Ishii&Zuber and hybrid models predict approximately the same void fraction, and the Brucato model does not provide better results than these two models.



331

332
333

Figure 11: Comparison of cross-sectional averaged void fraction for different eddy dissipation limits for the test 072.

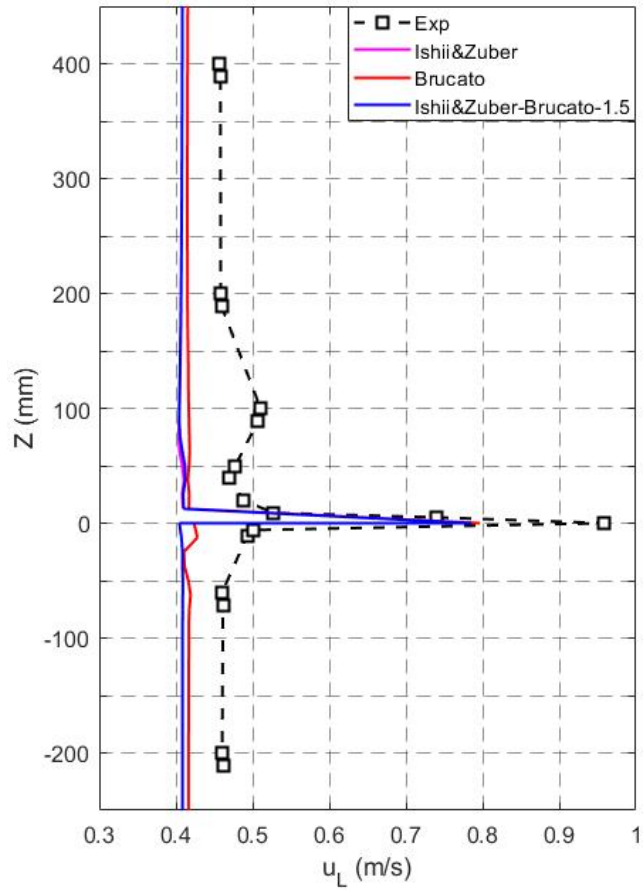


334

335
336

Figure 12: Radial void fraction distribution for Ishii&Zuber, Brucato and hybrid model for different axial positions for the test 072.

337



338

339

Figure 13: Cross-sectional averaged liquid velocity for the test 072.

340

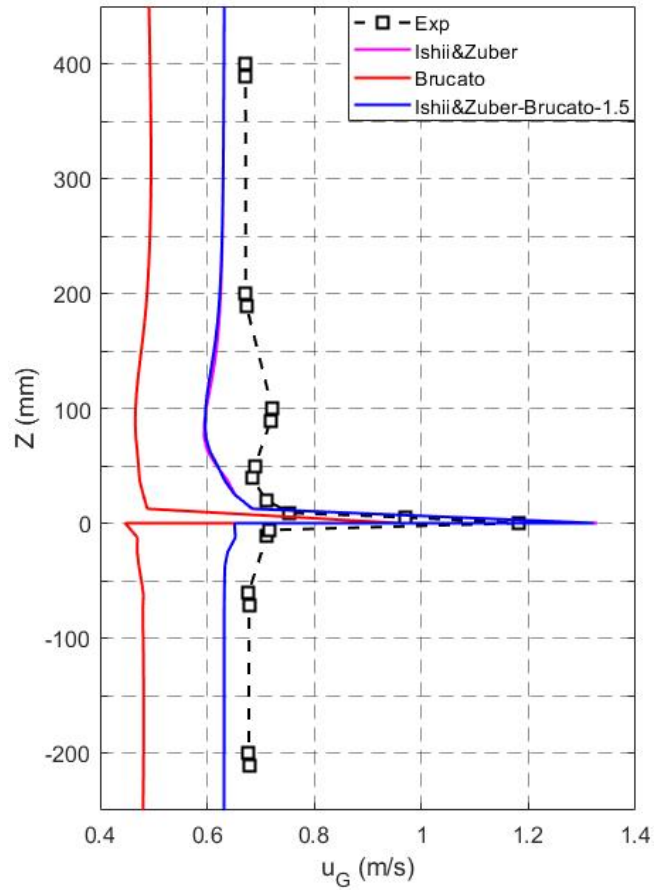
341

342

343

344

Figure 13 shows the averaged liquid velocity along the axial direction for the test case 072. As can be seen from the figure, all the drag models underestimate the velocity compared to the experiments at all Z positions. The Brucato model provides a slightly better liquid velocity prediction. Yet, the difference is very small. The averaged axial gas velocity is shown in Figure 14. The Ishii&Zuber and hybrid models predict the gas velocity better than the Brucato model.



345

346

Figure 14: Cross-sectional averaged gas velocity for the test 072.

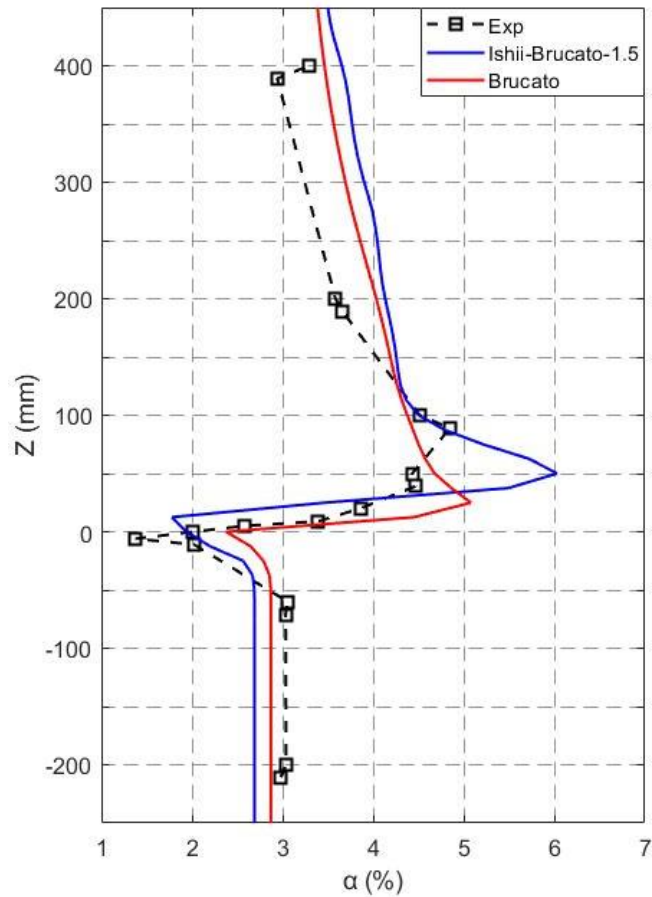
347

348

349

350

Considering the test case 074, Figure 15 shows the comparison of averaged void fraction for the Brucato and hybrid models. Although the Brucato model predicts the void fraction except in $-50 \text{ mm} < X < 150 \text{ mm}$ slightly better compared to the hybrid model, the hybrid model improves the prediction compared to Brucato in this region.



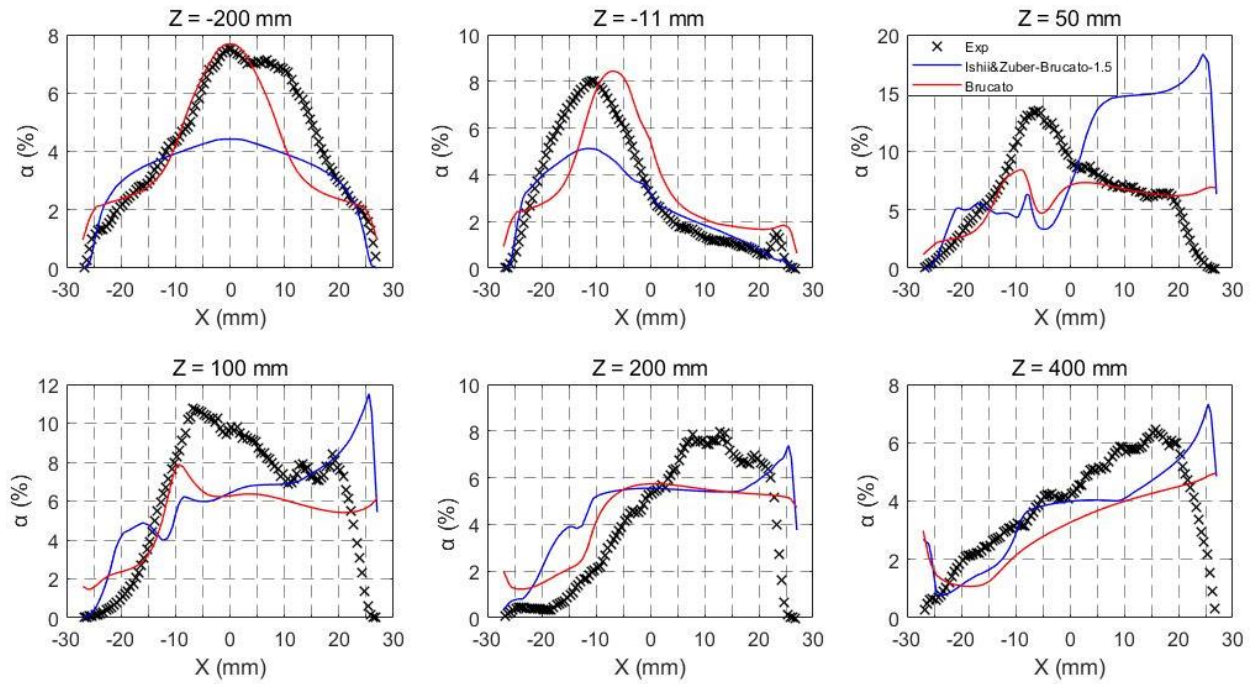
351

352
353

Figure 15: Comparison of cross-sectional averaged void fraction along the axial direction for Ishii&Zuber, Brucato and hybrid model for test 074.

354
355
356
357
358
359
360
361
362
363
364

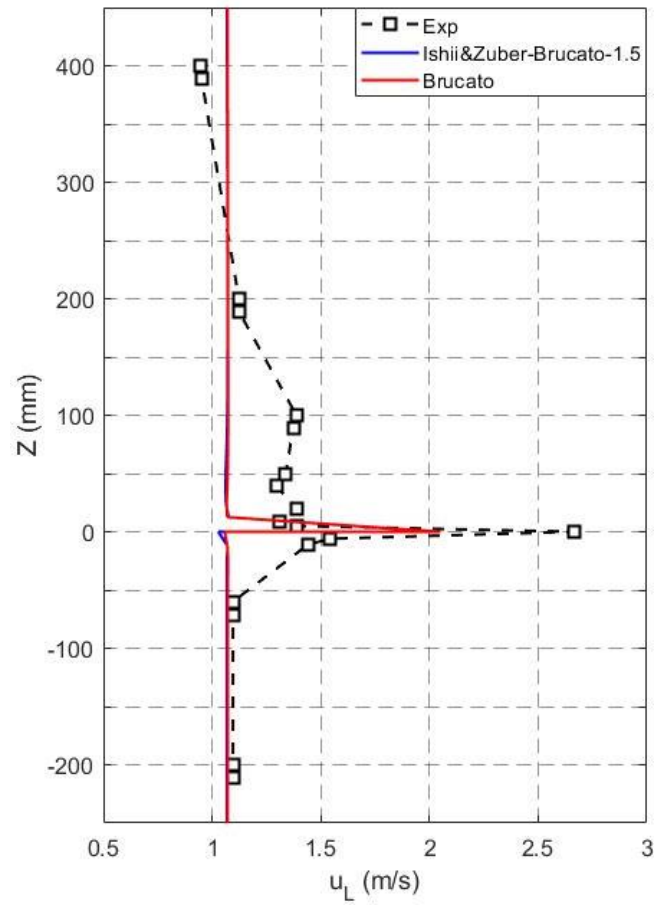
The radial void distribution for the Brucato and hybrid model is shown in Figure 16. For $Z = -200$ mm, the Brucato model predicts the void fraction well except in $5 \text{ mm} < X < 20$ mm while the hybrid model predicts well near the wall. For $Z = -11$ mm, the Brucato model generally predicts the void distribution better. For $Z = 50$ mm, the Brucato model estimations agree better with the experiments here while the hybrid model largely overestimates the void fraction on the right hand side of the pipe. For $Z = 100$ mm, the hybrid model provides a better prediction between $0 < X < 20$ mm whereas the Brucato model provides a better prediction between $-20 \text{ mm} < X < -5$ mm. For $Z = 200$ mm and $Z = 400$ mm, the hybrid and Brucato models provide similar void fraction distributions. For $Z = 200$ mm, they overestimate the void fraction between $-27 \text{ mm} < X < 0$ whereas they underestimate it between $0 < X < 20$ mm. For $Z = 400$ mm, they underestimate the void fraction between $-20 \text{ mm} < X < 20$ mm (except between $-10 \text{ mm} < X < 0$ for the hybrid model).



365

366 Figure 16: Radial void fraction distribution for Brucato and hybrid model for different axial positions for the test
 367 074.

368 Figure 17 and 18 show the averaged liquid and gas velocities for the test 074 respectively. As it can be
 369 seen in Figure 17, all models provide approximately the same liquid velocity prediction. Whereas the
 370 prediction agrees well with the experiments at downstream the obstacle, it is underestimated up to
 371 $Z = 200$ mm. The liquid velocity changes in the vortex region cannot be accurately estimated
 372 independent of the drag model by simulations. As shown in Figure 18, the hybrid model predicts the gas
 373 velocity well compared to the experiments downstream the obstacle. However, the Brucato model
 374 moderately underestimates it here. As for the liquid velocity, both models cannot capture the velocity
 375 changes at the obstacle downstream adequately.



376

377

Figure 17: Cross-sectional averaged liquid velocity for the test 074.

378

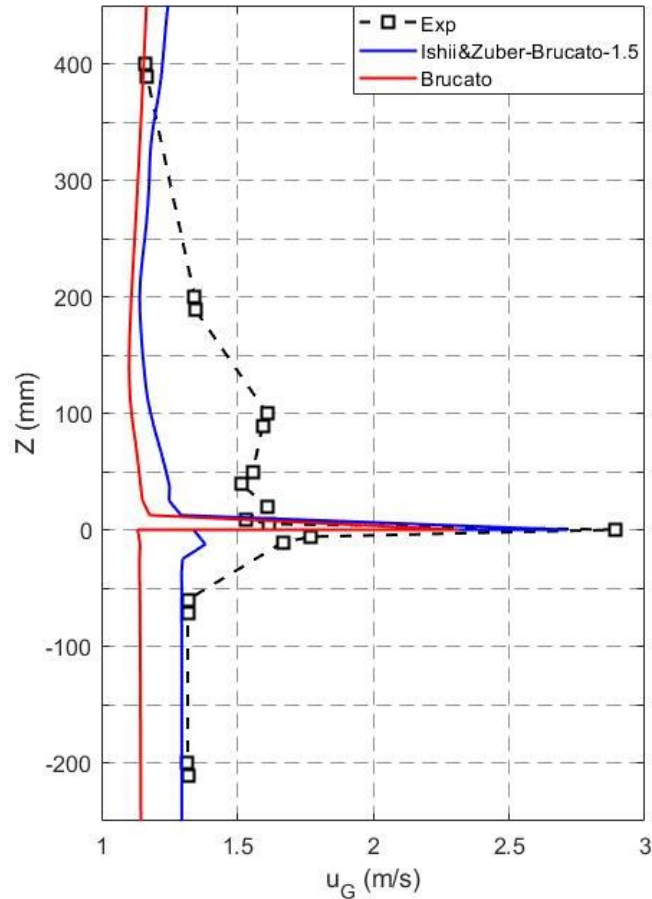


Figure 18: Cross-sectional averaged gas velocity for the test 074.

379

380

381

382 5. Conclusions

383 In this study, we examined the capability of different drag models for disperse gas-liquid flow at two
 384 different turbulence conditions for the case of an obstacle in a pipe that produces a pronounced vortex
 385 region. The Feng model underestimates the void fraction compared to the experiments for the low-
 386 velocity case for both the upstream (lower turbulence) and downstream (higher turbulence-vortex)
 387 region of the obstacle. This is attributed to the fact that this model is purely based on the Tomiyama
 388 model which holds for pure liquid (without contamination) systems. In addition, the simulations with
 389 the Feng model for the high-velocity case were highly unstable and no results could be obtained. The
 390 Bakker model moderately overestimates the void fraction compared to the experiments upstream of the
 391 obstacle for the low-velocity case. However, it extremely overestimates the void fraction downstream
 392 of the obstacle, especially in the vortex region. One reason may be that the bubble Reynolds number in
 393 the Bakker model has been formulated differently than other models. The coefficient used for the
 394 turbulent viscosity may not be applicable in the case of high turbulence.

395 For the low-velocity and high-velocity cases, the Grace model, the Tomiyama model, the Ishii&Zuber
 396 model, the Schiller&Naumann model, the Salibindla model and the Brucato model predict the void
 397 fraction well. It is attributed to the fact that neither turbulence nor bubble deformation are significant
 398 here. Thus, these models provide good void fraction predictions independent of whether or not the
 399 turbulence and/or bubble deformation effects are taken into account. However, the difference between
 400 low- and high-velocity cases appears downstream of the obstacle in the vortex region. For the low-
 401 velocity case, the Schiller&Naumann model, the Tomiyama model and the Grace model highly

402 overestimate the void fraction. The Ishii&Zuber model, which uses a slightly different definition
403 compared to Eq. 7 and the Salibindla model that includes a turbulence eddy dissipation correction,
404 provide the best void prediction here. Yet, the Brucato model is the only model that captures the void
405 peak. For the high-velocity case, all the models largely overestimate the void fraction, except the Brucato
406 model. Based on these findings, we concluded that in the presence of a vortex region with high eddy
407 dissipation changes, the drag model that considers the only bubble deformation is not sufficient.
408 Furthermore, the turbulence effect should be accounted for when the eddy dissipation exceeds a limit
409 value of ($\varepsilon_L = 1.5 \text{ m}^2 \text{ s}^{-3}$). Consequently, we propose a hybrid drag model depending on the eddy
410 dissipation limit, which improves the void fraction prediction.

411 We found that liquid and gas velocities are generally underpredicted for the low-velocity case compared
412 to the experimental data. However, the Brucato model provides less accurate gas velocity prediction
413 compared to the Ishii&Zuber and hybrid models. For the high-velocity case, where the Brucato and
414 hybrid models provide similar liquid velocity estimations upstream, the hybrid model predicts better the
415 gas velocity. Both models generally underestimate the gas and liquid velocities downstream.

416 As consequence, the influence of turbulence on the bubbles through the drag coefficient closure
417 improved the void fraction predictions, especially for high turbulent flow. Thus, it can be concluded that
418 the effects of turbulent eddies on drag force are needed to be considered for CFD modelling. Another
419 point is that it is still necessary to improve the gas and liquid velocity predictions, especially for
420 downstream. The explanation of gas and liquid velocity underestimation may be due to insufficient
421 turbulence modelling. Instead of using a two-equation model, using an advanced turbulence model like
422 the Reynolds Stress Model may improve the velocity predictions in the vortex region.

423 **References**

- 424 Asad, A., Kratzsch, C., & Schwarze, R. (2017). Influence of drag closures and inlet conditions on
425 bubble dynamics and flow behavior inside a bubble column. *Engineering Applications of*
426 *Computational Fluid Mechanics*, 11(1), 127-141. Retrieved from <Go to
427 ISI>://WOS:000388586200005. doi:10.1080/19942060.2016.1249410
- 428 Auton, T. R., Hunt, J. C. R., & Prudhomme, M. (1988). The Force Exerted on a Body in Inviscid
429 Unsteady Non-Uniform Rotational Flow. *Journal of Fluid Mechanics*, 197, 241-257.
430 doi:10.1017/S0022112088003246
- 431 Bakker, A., & Vandenakker, H. E. A. (1994). A Computational Model for the Gas-Liquid Flow in
432 Stirred Reactors. *Chemical Engineering Research & Design*, 72(A4), 594-606. Retrieved from
433 <Go to ISI>://WOS:A1994PE66500013.
- 434 Besagni, G., Guedon, G. R., & Inzoli, F. (2018). Computational fluid-dynamic modeling of the mono-
435 dispersed homogeneous flow regime in bubble columns. *Nuclear Engineering and Design*,
436 331, 222-237. doi:10.1016/j.nucengdes.2018.03.003
- 437 Brucato, A., Grisafi, F., & Montante, G. (1998). Particle drag coefficients in turbulent fluids. *Chemical*
438 *Engineering Science*, 53(18), 3295-3314. Retrieved from <Go to
439 ISI>://WOS:000076195300009. doi:Doi 10.1016/S0009-2509(98)00114-6
- 440 Burns, A. D., Frank, T., Hamill, I., & Shi, J.-M. (2004). *The Favre averaged drag model for turbulent*
441 *dispersion in Eulerian multi-phase flows*. Paper presented at the 5th International Conference
442 on Multiphase Flow, ICMF, Yokohama, Japan.
- 443 Chen, P. (2004). *Modeling the fluid dynamics of bubble column flows*. (Ph.D. Thesis), Sever Institute
444 of Washington University,
- 445 Doroodchi, E., Evans, G. M., Schwarz, M. P., Lane, G. L., Shah, N., & Nguyen, A. (2008). Influence
446 of turbulence intensity on particle drag coefficients. *Chemical Engineering Journal*, 135(1-2),
447 129-134. Retrieved from <Go to ISI>://WOS:000251593300018.
448 doi:10.1016/j.cej.2007.03.026
- 449 Feng, J., & Bolotnov, I. (2016). *Single bubble drag force evaluation in turbulent flow based on DNS*
450 *result*. Paper presented at the ANS Winter Meeting, Las Vegas, NV.

451 Grace, J. R., Wairegi, T., & Nguyen, T. H. (1976). Shapes and Velocities of Single Drops and Bubbles
452 Moving Freely through Immiscible Liquids. *Transactions of the Institution of Chemical*
453 *Engineers*, 54(3), 167-173. Retrieved from <Go to ISI>://WOS:A1976CD39200004.

454 Guan, X. P., Li, X. J., Yang, N., & Liu, M. Y. (2020). CFD simulation of gas-liquid flow in stirred
455 tanks: Effect of drag models. *Chemical Engineering Journal*, 386. Retrieved from <Go to
456 ISI>://WOS:000551293900003. doi:ARTN 121554
10.1016/j.cej.2019.04.134

457
458 Gupta, A., & Roy, S. (2013). Euler-Euler simulation of bubbly flow in a rectangular bubble column:
459 Experimental validation with Radioactive Particle Tracking. *Chemical Engineering Journal*,
460 225, 818-836. Retrieved from <Go to ISI>://WOS:000321313800094.
461 doi:10.1016/j.cej.2012.11.012

462 Hosokawa, S., Tomiyama, A., Misaki, S., & Hamada, T. (2002). *Lateral migration of single bubbles*
463 *due to the presence of wall*. Paper presented at the Proceedings of the ASME Joint U.S.-
464 European Fluids Engineering Division Conference, FEDSM2002, Montreal, Canada.

465 Ishii, M., & Zuber, N. (1979). Drag Coefficient and Relative Velocity in Bubbly, Droplet or
466 Particulate Flows. *Aiche Journal*, 25(5), 843-855. Retrieved from <Go to
467 ISI>://WOS:A1979HN38300012. doi:DOI 10.1002/aic.690250513

468 Jiang, X. D., Yang, N., & Yang, B. L. (2016). Computational fluid dynamics simulation of
469 hydrodynamics in the riser of an external loop airlift reactor. *Particuology*, 27, 95-101.
470 Retrieved from <Go to ISI>://WOS:000378959000011. doi:10.1016/j.partic.2015.05.011

471 Jin, D., Xiong, J. B., & Cheng, X. (2019). Investigation on interphase force modeling for vertical and
472 inclined upward adiabatic bubbly flow. *Nuclear Engineering and Design*, 350, 43-57.
473 doi:10.1016/j.nucengdes.2019.05.005

474 Karimi, M., Akdogan, G., Dellimore, K. H., & Bradshaw, S. M. (2012). *Comparion of different drag*
475 *coefficient correlations in the CFD modelling of a laboratory-scale Rushton-turbine flotation*
476 *tank*. Paper presented at the NInth International Conference on CFD in the Minerals and
477 Process Industries, CSIRO, Melbourne, Australia.

478 Khopkar, A. R., & Ranade, V. V. (2006). CFD simulation of gas-liquid stirred vessel: VC, S33, and
479 L33 flow regimes. *Aiche Journal*, 52(5), 1654-1672. Retrieved from <Go to
480 ISI>://WOS:000237128700003. doi:10.1002/aic.10762

481 Lane, G. L., Schwarz, M. P., & Evans, G. M. (2002). Predicting gas-liquid flow in a mechanically
482 stirred tank. *Applied Mathematical Modelling*, 26(2), 223-235. Retrieved from <Go to
483 ISI>://WOS:000174309600009. doi:Pii S0307-904x(01)00057-9
Doi 10.1016/S0307-904x(01)00057-9

484
485 Lane, G. L., Schwarz, M. P., & Evans, G. M. (2005). Numerical modelling of gas-liquid flow in
486 stirred tanks. *Chemical Engineering Science*, 60(8-9), 2203-2214. Retrieved from <Go to
487 ISI>://WOS:000227864000010. doi:10.1016/j.ces.2004.11.046

488 Liao, Y. X., Ma, T., Liu, L., Ziegenhein, T., Krepper, E., & Lucas, D. (2018). Eulerian modelling of
489 turbulent bubbly flow based on a baseline closure concept. *Nuclear Engineering and Design*,
490 337, 450-459. doi:10.1016/j.nucengdes.2018.07.021

491 Liao, Y. X., Rzehak, R., Lucas, D., & Krepper, E. (2015). Baseline closure model for dispersed bubbly
492 flow: Bubble coalescence and breakup. *Chemical Engineering Science*, 122, 336-349.
493 doi:10.1016/j.ces.2014.09.042

494 Ma, T., Santarelli, C., Ziegenhein, T., Lucas, D., & Frohlich, J. (2017). Direct numerical simulation-
495 based Reynolds-averaged closure for bubble-induced turbulence. *Physical Review Fluids*,
496 2(3). doi:10.1103/PhysRevFluids.2.034301

497 Masood, R. M. A., & Delgado, A. (2014). Numerical investigation of the interphase forces and
498 turbulence closure in 3D square bubble columns. *Chemical Engineering Science*, 108, 154-
499 168. Retrieved from <Go to ISI>://WOS:000332392100015. doi:10.1016/j.ces.2014.01.004

500 Menter, F. R. (1994). 2-Equation Eddy-Viscosity Turbulence Models for Engineering Applications.
501 *Aiaa Journal*, 32(8), 1598-1605. doi:10.2514/3.12149

502 Morsi, S. A., & Alexander, A. J. (1972). Investigation of Particle Trajectories in 2-Phase Flow
503 Systems. *Journal of Fluid Mechanics*, 55(Sep26), 193-+. Retrieved from <Go to
504 ISI>://WOS:A1972N745700001. doi:Doi 10.1017/S0022112072001806

505 Neumann-Kipping, M., Bieberle, A., & Hampel, U. (2020). Investigations on bubbly two-phase flow
506 in a constricted vertical pipe. *International Journal of Multiphase Flow*, 130.
507 doi:10.1016/j.ijmultiphaseflow.2020.103340

508 Pourtousi, M., Sahu, J. N., & Ganesan, P. (2014). Effect of interfacial forces and turbulence models on
509 predicting flow pattern inside the bubble column. *Chemical Engineering and Processing-
510 Process Intensification*, 75, 38-47. Retrieved from <Go to ISI>://WOS:000331924000005.
511 doi:10.1016/j.cep.2013.11.001

512 Salibindla, A. K. R., Masuk, A. U. M., Tan, S. Y., & Ni, R. (2020). Lift and drag coefficients of
513 deformable bubbles in intense turbulence determined from bubble rise velocity. *Journal of
514 Fluid Mechanics*, 894. Retrieved from <Go to ISI>://WOS:000530307300001. doi:ARTN
515 A20
10.1017/jfm.2020.244

516 Schiller, L., & Naumann, A. (1935). A drag coefficient correlation. *Z. Ver. Deutsch. Ing.* 77, 318-320.

517 Silva, M. K., d'Avila, M. A., & Mori, M. (2012). Study of the interfacial forces and turbulence models
518 in a bubble column. *Computers & Chemical Engineering*, 44, 34-44. Retrieved from <Go to
519 ISI>://WOS:000306603600004. doi:10.1016/j.compchemeng.2012.04.007

520 Simonnet, M., Gentric, C., Olmos, E., & Midoux, N. (2007). Experimental determination of the drag
521 coefficient in a swarm of bubbles. *Chemical Engineering Science*, 62(3), 858-866. Retrieved
522 from <Go to ISI>://WOS:000243714900019. doi:10.1016/j.ces.2006.10.012

523 Tabib, M. V., Roy, S. A., & Joshi, J. B. (2008). CFD simulation of bubble column - An analysis of
524 interphase forces and turbulence models. *Chemical Engineering Journal*, 139(3), 589-614.
525 Retrieved from <Go to ISI>://WOS:000256652500019. doi:10.1016/j.cej.2007.09.015

526 Tas-Koehler, S., Lecrivain, G., Krepper, E., Unger, S., & Hampel, U. (2020). Numerical investigation
527 on the effect of transversal fluid field deformation on heat transfer in a rod bundle with mixing
528 vanes. *Nuclear Engineering and Design*, 361. doi:10.1016/j.nucengdes.2020.110575

529 Tas-Koehler, S., Neumann-Kipping, M., Liao, Y. X., Krepper, E., & Hampel, U. (2021). CFD
530 simulation of bubbly flow around an obstacle in a vertical pipe with a focus on breakup and
531 coalescence modelling. *International Journal of Multiphase Flow*.
532 doi:doi.org/10.1016/j.ijmultiphaseflow.2020.103528

533 Tomiyama, A., Kataoka, I., Zun, I., & Sakaguchi, T. (1998). Drag coefficients of single bubbles under
534 normal and micro gravity conditions. *Jsm International Journal Series B-Fluids and Thermal
535 Engineering*, 41(2), 472-479. doi:10.1299/jsmeb.41.472

536 Tomiyama, A., Tamai, H., Zun, I., & Hosokawa, S. (2002). Transverse migration of single bubbles in
537 simple shear flows. *Chemical Engineering Science*, 57(11), 1849-1858. doi:10.1016/S0009-
538 2509(02)00085-4

539 Wang, Q. G., & Yao, W. (2016). Computation and validation of the interphase force models for
540 bubbly flow. *International Journal of Heat and Mass Transfer*, 98, 799-813. Retrieved from
541 <Go to ISI>://WOS:000375360600075. doi:10.1016/j.ijheatmasstransfer.2016.03.064

542 Yamoah, S., Martinez-Cuenca, R., Monros, G., Chiva, S., & Macian-Juan, R. (2015). Numerical
543 investigation of models for drag, lift, wall lubrication and turbulent dispersion forces for the
544 simulation of gas-liquid two-phase flow. *Chemical Engineering Research & Design*, 98, 17-
545 35. Retrieved from <Go to ISI>://WOS:000356755500002. doi:10.1016/j.cherd.2015.04.007

546 Yeoh, G. H., & Tu, J. Y. (2009). *Computational Techniques for Multiphase Flows*: Butterworth-
547 Heinemann.

548 Zhang, D., Deen, N. G., & Kuipers, J. A. M. (2006). Numerical simulation of the dynamic flow
549 behavior in a bubble column: A study of closures for turbulence and interface forces.
550 *Chemical Engineering Science*, 61(23), 7593-7608. Retrieved from <Go to
551 ISI>://WOS:000242486500003. doi:10.1016/j.ces.2006.08.053

552 Zhang, D. Z., & VanderHeyden, W. B. (2002). The effects of mesoscale structures on the macroscopic
553 momentum equations for two-phase flows. *International Journal of Multiphase Flow*, 28(5),
554 805-822. Retrieved from <Go to ISI>://WOS:000175820800006. doi:Pii S0301-
555 9322(02)00005-8

556 Doi 10.1016/S0301-9322(02)00005-8

Declaration of Interest Statement

02.04.2021

Dear Editor,

The authors certify that they have no affiliations or involvement in any organization or entity with any financial interest or non-financial interest in the subject matter or materials discussed in this manuscript.

We confirm that this work is original and has not been published elsewhere, nor is it currently under consideration for publication elsewhere.

Sincerely,

Sibel Tas-Koehler